# A design strategy in the propulsion system attachment to a submarine hull to minimise radiated noise

## Mauro Caresta, Nicole Kessissoglou

School of Mechanical and Manufacturing Engineering, The University of New South Wales, Sydney, NSW 2052, Australia

## ABSTRACT

Vibration modes of a submerged hull are excited by fluctuating forces generated at the propeller and transmitted to the hull via the propeller-shafting system. The low frequency hull vibrational modes result in significant sound radiation. This work investigates the reduction of the far-field radiated sound pressure by optimising the connection point of the shafting system to the hull. The submarine hull is modelled as a fluid loaded cylindrical hull with truncated conical shells at each end. The propeller-shafting system consists of the propeller, shaft, thrust bearing and foundation, and is modelled in a modular approach using a combination of spring-mass-damper elements and continuous systems (beams, plates, shells). The foundation is attached to the stern side end plate of the hull, which is modelled as a circular plate coupled to an annular plate. By tuning the connection radius of the foundation to the end plate, the maximum radiated noise in a given frequency range can be minimised.

## INTRODUCTION

Rotation of the propeller in a spatially non uniform wake results in fluctuating forces generated at the propeller blade passing frequency (Lewis, 1988). This low frequency harmonic excitation is transmitted to the submarine hull via the propeller-shafting system. Many researchers have investigated ways of reducing the transmission of harmonic forces to the hull by modifying the dynamic response of the propeller-shafting system (Kane and McGoldrick, 1949; Rigby, 1948; Schwanecke, 1979 ). Rigby (1948) showed that reduction of the axial vibrations could be achieved by increasing the number of blades on the propeller. Parkins and Horner (1989) presented an active magnetic feedback control method to reduce the axial vibrations of a submarine shaft. Goodwin (1960) examined the reduction of axial vibration transmitted through the propeller-shafting system by means of a resonance changer, using a simplified spring-mass model of the propeller-shafting system with a rigid termination. A dynamic model of a submarine hull in axisymmetric motion was coupled with a dynamic model of a propeller-shafting system, in order to determine the optimum resonance changer parameters from minimisation of the hull drive point velocity and structure-borne radiated sound pressure (Dylejko, 2007). The radiated sound power with and without the use of a resonance changer was also investigated by Merz et al. (2009), using a coupled FE/BE model for axisymmetric motion and considering the hull under both structural and dipole excitation due to the propeller. Pan et al. (2008a, 2008b) used active control strategies to attenuate the low frequency hull radiated noise using an axisymmetric submarine hull model.

A semi-analytical model has been presented previously by the authors to predict the radiated sound pressure of a submerged vessel under harmonic excitation in both the axial and radial directions (Caresta and Kessissoglou, 2010). The model was shown to give reliable results in the low frequency range but did not include the full dynamic of a propeller-shafting system. In this work, a dynamic model of the propeller-shafting system is coupled with the hull dynamic model presented by Caresta and Kessissoglou (2010) for axisymmetric motion only. The connection radius of the attachment between the propeller-shafting system and the hull is tuned in an attempt to minimise the radiated sound pressure. The flexibility of the end plate at the coupling between the propeller-shafting system and hull is taken into account. Results show that the location where the shafting system is attached to the hull is shown to have a great influence on the structural and acoustic responses of the submarine, due to the change in force transmissibility between the propeller-shafting system and the hull. The optimum radius of the propeller-shafting system connection to the hull is found by directly minimising the far-field radiated sound pressure. It is shown that the connection radius can be used as a tuning parameter to minimise a cost function in a wide frequency range or at discrete frequencies.

## DYNAMIC MODEL OF THE SUBMARINE

The submarine hull is modelled as a cylindrical shell with internal bulkheads and ring stiffeners, and truncated conical shells at each end. The cones are closed at each end by circular plates, as shown in Figure 1. The entire structure is submerged in a heavy fluid medium.
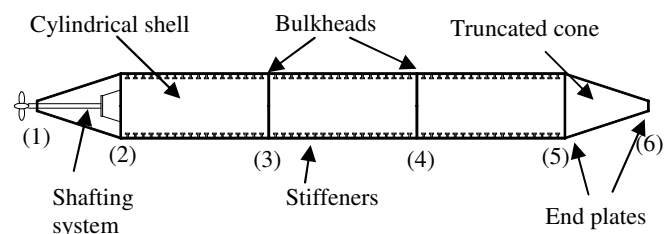


**Figure 1**. Schematic diagram of the submarine

The propeller-shafting system is located at the stern side of the submarine. The propulsion forces generated by the fluctuating forces at the propeller are transmitted to a thrust bearing located along the main shaft. The thrust bearing is connected to the foundation, which in turn is attached to the stern side end plate. A schematic diagram of the propeller-shafting system is shown in Figure 2. The end plate is modelled as a circular plate coupled to an annular plate, and the annular plate is attached to the cylindrical hull.
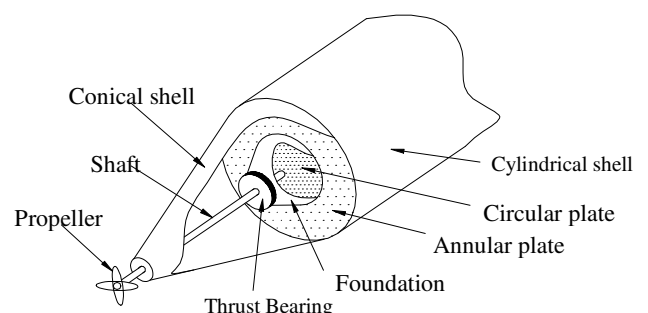


**Figure 2**. Schematic diagram of the shafting system

## Cylindrical shell

The fluctuating forces generated at the propeller, arising from the rotation of the propeller through a non-uniform wake field, are transmitted through the propeller-shafting system and result in axial excitation of the hull. A detailed dynamic model of the submarine hull under axial and radial harmonic excitation has been previously presented by the authors (Caresta and Kessissoglou, 2010). This model is briefly reviewed here for axisymmetric motion, and then coupled to a dynamic model of the propeller-shafting system. Flügge equations of motion were used to model the cylindrical shell. T-shaped stiffeners were dynamically included using smeared theory (Hoppmann, 1958). Only axisymmetric motion is considered, hence the circumferential displacement for the zeroth circumferential mode number becomes decoupled from the equations of motion for the axial and radial displacements. Since the displacement of the surrounding fluid due to the hull torsional displacement does not significantly contribute to sound radiation, the circumferential displacement is not considered further. In Figure 3, $u$ and $w$ are the orthogonal components of displacement in the $x$ and $z$ directions, respectively. $a$ is the mean radius of the cylindrical shell, $h$ is the shell thickness and $\phi = \partial w / \partial x$ is the slope.
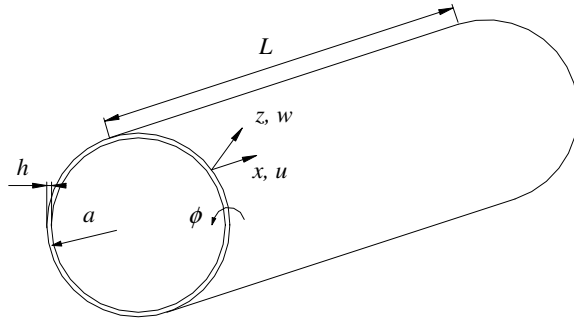


**Figure 3**. Cylindrical shell in axisymmetric motion

The Flügge equations of motion for axisymmetric motion of a ring-stiffened fluid-loaded cylindrical shell are given by (Rosen and Singer, 1974)

$$\frac{\partial^2 u}{\partial x^2} + \frac{v}{a}\frac{\partial w}{\partial x} - \beta^2 a \frac{\partial^3 w}{\partial x^3} - \frac{\gamma}{c_L^2}\frac{\partial^2 u}{\partial t^2} = 0 \tag{1}$$

$$\frac{v}{a}\frac{\partial u}{\partial x} - \beta^2 a \frac{\partial^3 u}{\partial x^3} + d_6 w + \beta^2\left(d_8 w + a^2 \frac{\partial^4 w}{\partial x^4}\right) + \frac{\gamma}{c_L^2}\frac{\partial^2 w}{\partial t^2} - \frac{p}{\rho h c_L^2} = 0 \tag{2}$$

$E$, $\rho$ and $v$ are respectively the Young's modulus, density and Poisson's ratio of the cylinder. $c_L = [E / \rho(1-v^2)]^{1/2}$ is the longitudinal wave speed and $p$ is the external pressure due to the surrounding seawater and can be written in term of an acoustic impedance $Z$ by

$$p = Z\dot{w} = \frac{j\rho h c_L^2}{\omega a^2} F_L \dot{w} \tag{3}$$

The fluid loading term $F_L$ in Eq. (3) is given by Fuller (1986). The coefficients $\beta$, $q_1$, $q_2$ and $d_i$ for $i=6,8$ are given in accordance with Caresta and Kessissoglou (2010). The axial and radial displacements for the cylindrical shell can respectively be written as (Leissa, 1993)

$$u(x,t) = \sum_{i=1}^{6} C_i W_i e^{jk_i x} e^{-j\omega t} \tag{4}$$

$$w(x,t) = \sum_{i=1}^{6} W_i e^{jk_i x} e^{-j\omega t} \tag{5}$$

$k$ is the axial wavenumber, $j$ is the imaginary unit and $\omega$ is the angular frequency. $C_i = U_i / W_i$ is an amplitude ratio. $U_i$, $W_i$ are the wave amplitude coefficients of the axial and radial displacements, respectively.

## Circular plates

The end plates and bulkheads were modelled as thin circular plates in both in-plane and bending motion. The stern side end plate is modelled as an internal circular plate coupled to an annular plate. The axial $w_p$ and radial $u_p$ plate displacements in polar coordinates $(r,\theta_p)$ are shown in Figure 4. $\phi_p = \partial w_p / \partial r$ is the slope.
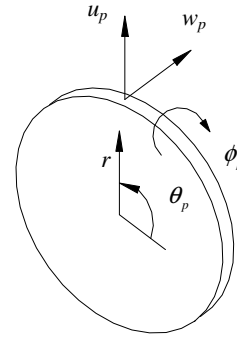


**Figure 4**. Thin circular plate in axisymmetric motion

For axisymmetric motion, the equations of motion are given by (Tso and Hansen, 1995)

$$\nabla^4 w_p + \frac{\rho_p h_p}{D_p}\frac{\partial^2 w_p}{\partial t^2} = 0 \tag{6}$$

$$\frac{\partial}{\partial r}\left(\frac{\partial u_p}{\partial r} + \frac{u_p}{r}\right) - \frac{1}{c_{pL}^2}\frac{\partial^2 u_p}{\partial t^2} = 0 \tag{7}$$

where $\nabla^4 = \nabla^2\nabla^2$ and $\nabla^2 = \frac{\partial^2}{\partial r^2} + \frac{1}{r}\frac{\partial}{\partial r}$ for axisymmetric motion. $h_p$ is the plate thickness. $D_p = E_p h_p^3(12 - v_p^2)$ is the flexural rigidity, where $E_p$, $\rho_p$ and $v_p$ are the Young's modulus, density and Poisson's ratio of the circular plate. $c_{pL} = [E_p / \rho_p(1-v_p^2)]^{1/2}$ is the longitudinal wave speed. General solutions for the axial and radial displacements (for both the full or annular plates) are respectively given by

$$w_p(r,t) = \left(A_1 J_0(k_{pB}r) + A_2 I_0(k_{pB}r) + A_3 Y_0(k_{pB}r) + A_4 K_0(k_{pB}r)\right)e^{-j\omega t} \tag{8}$$

$$u_p(r,t) = \left(B_1 \frac{\partial J_0(k_{pL}r)}{\partial r} + B_2 \frac{\partial Y_0(k_{pL}r)}{\partial r}\right)e^{-j\omega t} \tag{9}$$

$k_{pB}$ and $k_{pL}$ are the wavenumbers for bending and in-plane waves in the plate. $J_0$ and $I_0$ are respectively the Bessel function and the modified Bessel function of the first kind, $Y_0$ is Bessel of the second kind. The coefficients $A_i$ ($i=1:4$) and $B_i$ ($i=1:2$) are determined from the boundary conditions. For a full circular plate, $A_3$, $A_4$ and $B_2$ are zero.

## Conical end caps

The fluid loaded truncated conical shells were modelled by dividing the conical shells into narrow strips which were considered to be locally cylindrical. The narrow segments were coupled together by applying continuity equations at each interface. The fluid loading approximation was shown to be reliable at low frequencies. Details on the dynamic modelling of truncated conical shells under fluid loading can be found in Caresta and Kessissoglou (2008).

## Propeller-shafting system

The propeller-shafting system consists of the propeller, shaft, thrust bearing and foundation, and is modelled in a modular approach using a combination of spring-mass-damper elements and beam/shell systems. $M_{pr}$ is the mass of the propeller which is modelled as a lumped mass at the end of the shaft, as shown in Figure 5. The shaft is modelled as a rod in longitudinal vibration. The connection of the thrust bearing on the shaft is located at $x_{s1} = L_{s1}$. Hence, the shaft dynamic response is obtained by separating the shaft in two sections. The motion is described by coordinates $u_{s1}$ and $u_{s2}$ in the $x_{s1}$ and $x_{s2}$ directions, respectively. The equation of motion for a shaft in longitudinal vibration is given by

$$\frac{\partial^2 u_{si}(x_{si},t)}{\partial x_{si}^2} - \frac{1}{c_{sL}^2}\frac{\partial^2 u_{si}(x_{si},t)}{\partial t^2} = 0, \quad i=1,2 \qquad (10)$$

$c_{sL} = (E_s / \rho_s)^{1/2}$ is the longitudinal wave speed. The general solution for the longitudinal displacement for the two sections $i$ of the shaft is given by

$$u_{si}(x_{si},t) = (A_{si,1}e^{-k_s x_{si}} + A_{si,2}e^{k_s x_{si}})e^{-j\omega t}, \quad i=1,2 \qquad (11)$$

where $k_s = \omega / c_{sL}$ is the axial wavenumber of the shaft. At low frequencies, the thrust bearing dynamics can be modelled as a single degree of freedom system of mass $M_b$, stiffness $K_b$ and damping coefficient $C_b$. At low frequencies, the foundation can be considered rigid (Dylejko, 2007) and its dynamic effect is just an added mass $M_f$.
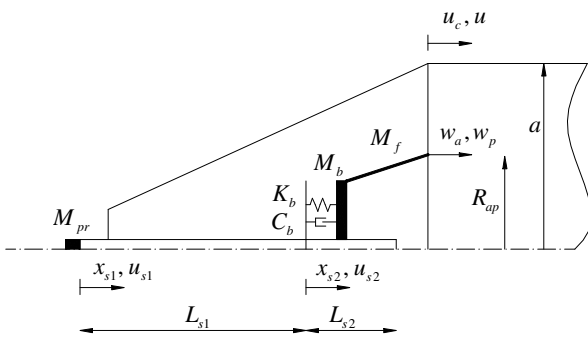


**Figure 5**. Displacements and coordinate system for the propeller-shafting system

## Boundary and continuity conditions for the hull

The dynamic response of the entire structure can be calculated by assembling the boundary conditions at each end of the coupled cylindrical-conical shell together with the continuity equations at the junctions of the cones, cylindrical

shell and bulkheads. The forces, moments, displacements and slope at the junctions and boundaries of the coupled shells and plates are given in accordance with the sign convention shown in Figure 6, where $RC_0$ is the global Cartesian reference frame. The membrane forces ($N_x$, $N_\theta$, $N_{x\theta}$), bending moments ($M_x$, $M_\theta$, $M_{x\theta}$), transverse shearing $Q_x$ and the Kelvin-Kirchhoff shear force $V_x$ for the cylindrical shells, conical shells and circular plates can be found in Leissa (1993) .

$u$, $v$ and $w$ are respectively the axial, circumferential and radial components of displacement for the cylindrical shell. $u_p$ and $w_p$ are respectively the radial and axial displacements of the circular plates. $u_a$ and $w_a$ are respectively the radial and axial displacements of the annular plate. $u_c$ and $w_c$ are the axial and radial components of displacement for the conical shell. To take into account the change of curvature between the cylinder and the cone, the following notation was introduced

$$\tilde{u}_c = u_c \cos\alpha - w_c \sin\alpha \qquad (12)$$

$$\tilde{w}_c = w_c \cos\alpha + u_c \sin\alpha \qquad (13)$$

$$\tilde{N}_{x,c} = N_{x,c}\cos\alpha - V_{x,c}\sin\alpha \qquad (14)$$

$$\tilde{V}_{x,c} = V_{x,c}\cos\alpha + N_{x,c}\sin\alpha \qquad (15)$$

At the cone/circular plate/cylinder junction corresponding to junction (2) in Figure 1, the eight continuity conditions are given by

$$u = \tilde{u}_c = w_a \qquad (16)$$

$$w = \tilde{w}_c = u_a \qquad (17)$$

$$-\phi = -\phi_c = \phi_a \qquad (18)$$

$$-N_x - \tilde{N}_{x,c} + N_{x,a} = 0 \qquad (19)$$

$$-M_x + M_{x,c} - M_{x,a} = 0 \qquad (20)$$

$$-V_x + \tilde{V}_{x,c} + N_{r,a} = 0 \qquad (21)$$

Similar equations are used at the cone/plate/cylinder junction corresponding to junction 5 in Figure 1, in which the displacement, slope, force and moment terms associated with the annular plate ($u_a$, $w_a$, $\phi_a$, $N_{x,a}$, $M_{x,a}$, $N_{r,a}$) are replaced with those for a full circular plate ($u_p$, $w_p$, $\phi_p$, $N_{x,p}$, $M_{x,p}$, $N_{r,p}$). At the cylindrical shell/circular plate junctions corresponding to junctions (3) and (4) in Figure 1, similar expressions for the continuity conditions can be used in which the conical shell terms are omitted. Likewise, at the free ends of the truncated cones corresponding to junctions (1) and (6) in Figure 1, similar expressions for the continuity conditions between the conical shells and circular plates can be used.
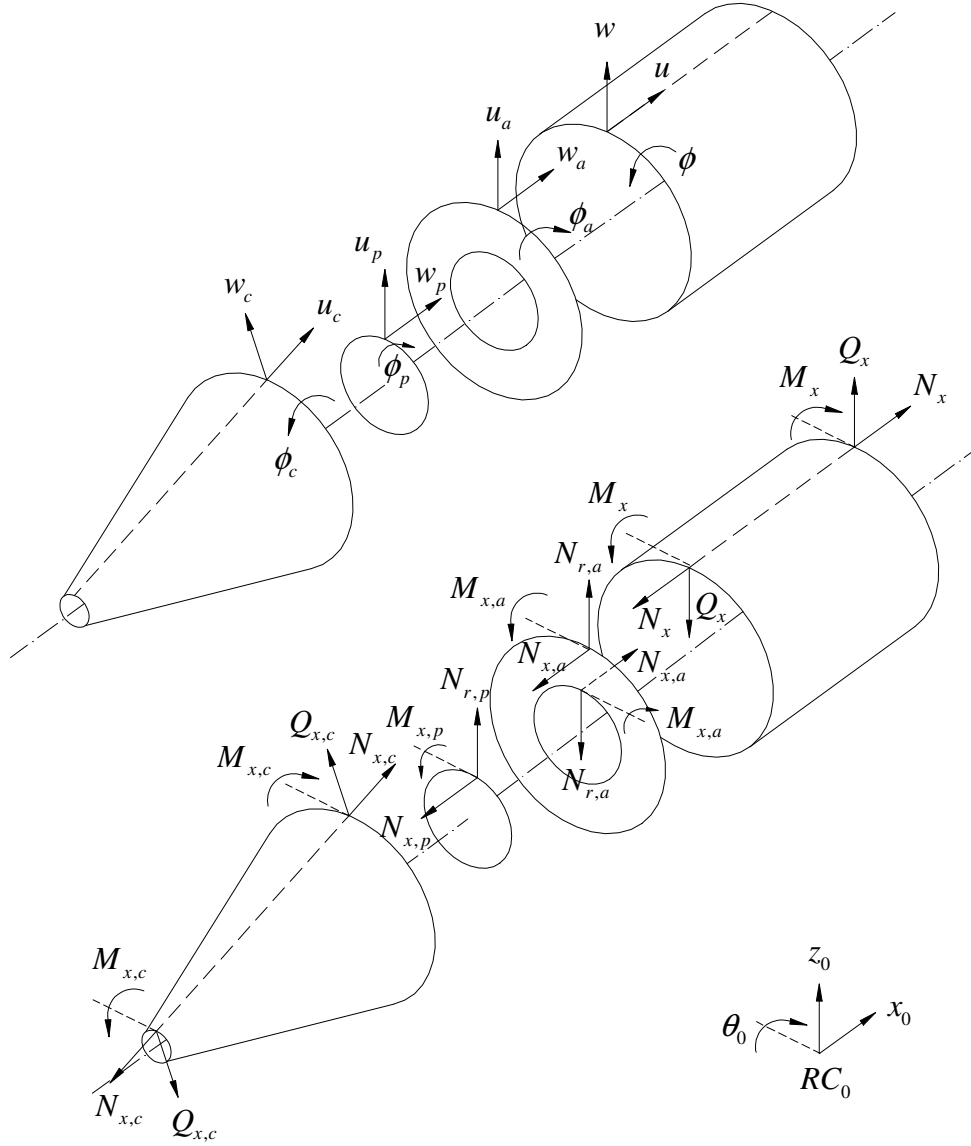
**Figure 6**. Sign convention for the forces, moments, displacements and slope

## Boundary and continuity conditions between the hull and propeller-shafting system

The boundary and continuity conditions for the shaft are given by

$$E_s A_s \frac{\partial u_{s1}(x_{s1})}{\partial x_{s1}} + \tilde{M}_{pr} \omega^2 u_{s1}(x_{s1}) = 0 \ , \ x_{s1} = 0 \tag{22}$$

$$E_s A_s \frac{\partial u_{s2}(x_{s2})}{\partial x_{s2}} = 0 \ , \ x_{s2} = L_{s2} \tag{23}$$

$$E_s A_s \frac{\partial u_{s1}(x_{s1})}{\partial x_{s1}} - E_s A_s \frac{\partial u_{s2}(x_{s2})}{\partial x_{s2}} - (K_b - j\omega C_b)[u_{s1}(x_{s1}) - w_p(r)] = 0,$$
$$x_{s1} = L_{s1}, \ x_{s2} = 0, \ r = R_{ap} \tag{24}$$

In Eq. (22), the mass of water $M_w$ displaced by the propeller is added to the propeller mass, resulting in $\tilde{M}_{pr} = M_{pr} + M_w$ (Merz et al., 2009). For the attachment location at $r = R_{ap}$, between the foundation of the propeller-shafting system and the hull stern side end plate, the boundary conditions are

$$N_{x,a}(r) - N_{x,p}(r) - (K_b - j\omega C_b)[w_p(r) - u_{s1}(x_{s1})]$$
$$+(M_b + M_f)\omega^2 w_p(r) = 0, \qquad x_{s1} = L_{s1} \tag{25}$$

$$w_a(r) = w_p(r) = u_{s1}(x_{s1}) \ , \qquad x_{s1} = L_{s1} \tag{26}$$

$$u_a(r) = u_p(r) = 0 \tag{27}$$

$$\phi_a(r) = \phi_p(r) = 0 \tag{28}$$

The boundary and continuity equations for the hull shells and plates, and between the hull and propeller-shafting system, can be arranged in matrix form $\mathbf{Bx} = \mathbf{0}$, where $\mathbf{x}$ is the vector of unknown coefficients. The vanishing of the determinant of $\mathbf{B}$ gives the natural frequencies of the system. The steady state response can be calculated using a direct method in which the force is considered as part of the boundary conditions. For a unitary harmonic force from the propeller, the boundary condition of the shaft corresponding to Eq. (22) becomes

$$E_s A_s \frac{\partial u_{s1}(x_{s1})}{x_{s1}} + \tilde{M}_{pr} \omega^2 u_{s1}(x_{s1}) = F_0 e^{-j\omega t} \ , \quad x_{s1} = 0 \tag{29}$$

The boundary and continuity equations can now be arranged in matrix form $\mathbf{Bx} = \mathbf{F}$. $\mathbf{F}$ is the force vector with only one non-zero element corresponding to $F_0$.

## FAR FIELD SOUND PRESSURE

A detailed acoustic model of the submarine has been previously presented by the authors (Caresta and Kessissoglou, 2010). The sound pressure at a far field location was solved by means of the Helmholtz integral formulation. The far field is located using spherical coordinates, as shown in Figure 7.
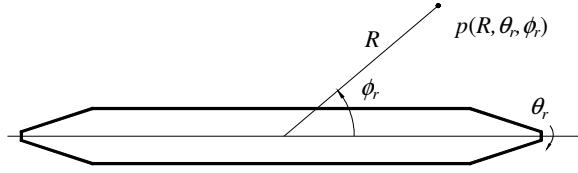
**Figure 7**. Coordinate system for the far field point.

## RESULTS

Results are presented for a ring stiffened steel cylinder of radius $a = 3.25$ m, thickness $h = 0.04$ m, length $L = 45$ m and with two evenly spaced bulkheads of thickness $h_p = 0.04$ m. To account for the onboard equipment and ballast tanks in the cylindrical section of the hull, a distributed mass on the shell of $m_{eq} = 1500 \, \mathrm{kgm^{-2}}$ has been considered (Tso and Jenkins, 2003). The internal stiffeners have a T cross-section and are evenly spaced by $b = 0.5$ m. The truncated conical shells at each end of the cylindrical hull have $R_1 = 0.50$ m, $R_2 = 3.25$ m, $\alpha = 18°$ and thickness $h_c = 0.014$ m. The thickness of the end plates is the same as for the bulkheads ( $h_p = 0.04$ m). The parameters for the propeller-shafting system are as follows: the propeller mass is $M_{pr} = 10^4$ kg and the mass of water displaced by the propeller is $M_w = 11443$ kg. The thrust bearing mass, stiffness and damping coefficient are $M_b = 200$ kg, $K_b = 2 \times 10^{10} \mathrm{Nm^{-1}}$ and $C_b = 3 \times 10^7$ kg/s, respectively. The two sections of the shaft are of length $L_{s1} = 9.0$ m and $L_{s2} = 1.5$ m.

All the structures are made of steel with density $\rho = 7800 \, \mathrm{kgm^{-3}}$, Young's modulus $E = 2.1 \times 10^{11} \, \mathrm{Nm^{-2}}$ and Poisson's ratio $\upsilon = 0.3$. Structural damping was introduced using a complex Young modulus $E = E(1 - j\eta)$, where $\eta = 0.02$ is the structural loss factor.

The frequency response function (FRF) of the axial displacement at junction 2 in Fig. 1 is shown in Fig. 8, for different values of the connection radius $R_{ap}$. The first three axial resonances of the hull are located at around 23, 45 and 70 Hz. The amplitudes at resonance are affected by the damping effect of the fluid loading and become smoother as the frequency increases. The lowest frequency peak is due to the resonance of the end plate and corresponds to large deformation of the annular plate. As the connection radius become larger, this resonance shifts to higher frequencies, increasing from 2.8 Hz for $R_{ap} = 0.5$ m to 14.7 Hz for $R_{ap} = 2.5$ m. Furthermore, for larger values of $R_{ap}$, the deformation of the inner circular plate increases. The dynamic behaviour of the end plate at the second resonance is more complex. For increasing values of $R_{ap}$, the resonant frequency increases and then decreases. The decrease in the

second resonant frequency occurs when the connection radius approaches the anti-nodes of the plate deformation, resulting in greater structural response. Other peaks in the FRFs at 9 and 36 Hz are due to the bulkhead resonances, and are unaffected by the shift of the connection radius. In general, as the connection radius increases and approaches the hull radius ( $R_{ap} \to a$ ), higher responses in the FRFs are observed. This is due to the fact that less energy is filtered by the transmissibility of the annular/circular plate system.
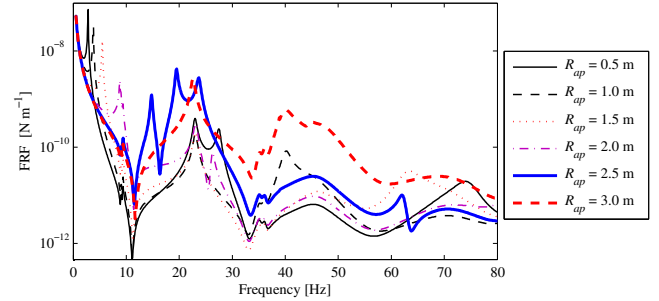
**Figure 8**. Frequency response function of the axial displacement for the cylinder at $x=0$ for different values of the connection radius.

The maximum sound pressure defined as $P_{\max} = \max\limits_{0 \le \phi_r \le 2\pi} p(R)$ at a far-field location of $R$=1000m is shown in Fig. 9 as a Sound Pressure Level (SPL) for different values of the connection radius $R_{ap}$, ranging from 0.5 m to 3.0 m. The sound radiation increases considerably as the connection radius becomes larger, especially in the medium frequency range, and is attributed to the increase in the structural response.
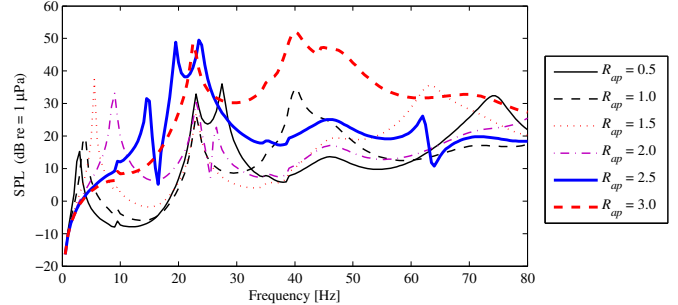
**Figure 9**. Maximum far field sound pressure at $R = 1000$m for different values of the connection radius

The optimum value for the connection radius $R_{ap}$ can be found minimising the overall value of the maximum sound pressure in the frequency range between zero and an upper value denoted by $f_u$. The cost function to be minimised is then defined as

$$J_{0-f_u} = \int_0^{f_u} P_{\max} df \qquad (30)$$

The overall maximum radiated sound for two frequency ranges using $f_u = 80$ Hz and $f_u = 40$ Hz are given in Figs. 10 and 11, respectively. The cost function can also be minimised at one or several discrete frequencies. In Fig. 12, the maximum radiated sound pressure ( $P_{\max}$ ) is minimised at the fundamental propeller *bpf* of 25 Hz. In Fig. 13, $P_{\max}$ is minimised at the fundamental *bpf* and its $n$ harmonics, scaled by $1/n$.

The optimum values for the connection radius for the various cost functions are highlighted in Figs. 10 to 13 with a black spot, and summarised in Table 1. The results for the maximum pressure using the optimum $R_{ap}$ values in Table 1 are shown in Figs. 14 to 17, and are compared with the result for a rigid connection to the pressure hull ( $R_{ap} = a$ ). For the case of minimising the cost function at a discrete frequency ( $J_{25}$ ), the optimum value for the connection radius results in an anti-resonance in the frequency response, as shown in Fig. 16. Figure 15 shows that as a result of minimising $J_{0-40}$, the maximum sound pressure is greater for frequencies above 40 Hz compared to the case of minimising the cost function for the full frequency range ( $J_{0-80}$ ) as shown in Fig. 14. Comparing Figs. 14 to 17, the best overall solution for both minimisation of the full frequency range (up to 80 Hz) and at the propeller *bpf* and its harmonics is given using a connection radius of around $R_{ap} = 0.8$ m.

Table 1. Optimum connection radius $R_{ap}$

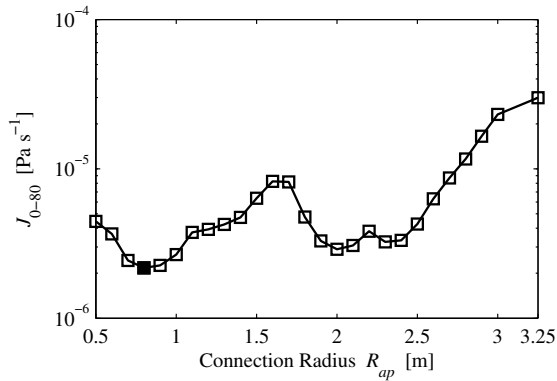| Cost function | $R_{ap}$ |
|---|---|
| $J_{0-80}$ | 0.8 m |
| $J_{0-40}$ | 1.3 m |
| $J_{25,50,75}$ | 0.9 m |
| $J_{25}$ | 2.0 m |



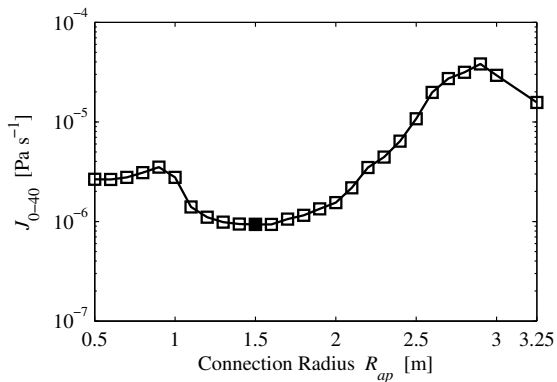Figure 10. Variation of the cost function $J_{0-80}$



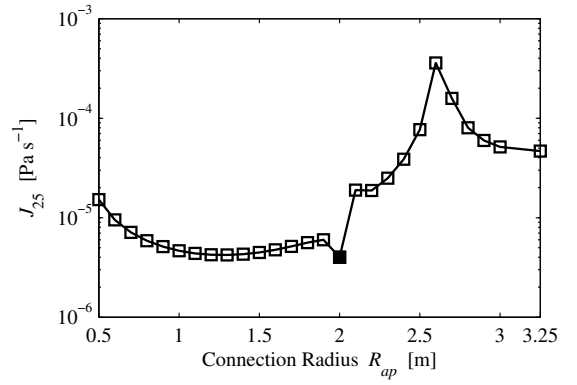Figure 11. Variation of the cost function $J_{0-40}$



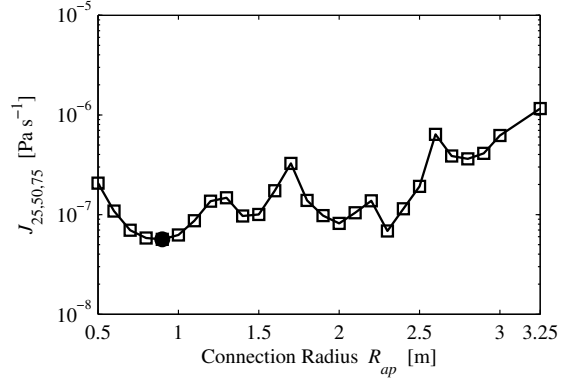Figure 12. Variation of the cost function $J_{25}$



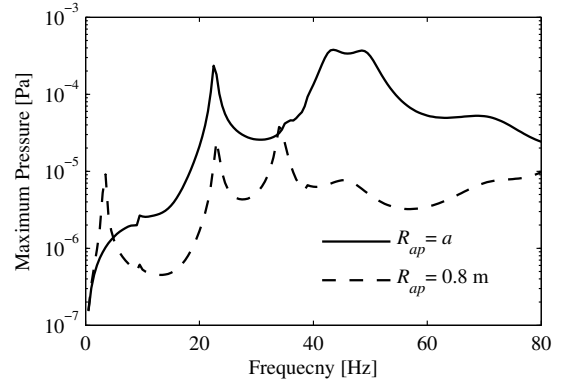Figure 13. Variation of the cost function $J_{25,50,75}$



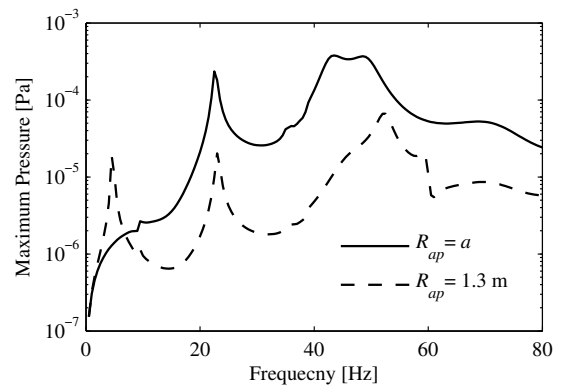Figure 14. Maximum sound pressure for the optimum value of $R_{ap}$ as a result of minimising $J_{0-80}$



Figure 15. Maximum sound pressure for the optimum value of $R_{ap}$ as a result of minimising $J_{0-40}$
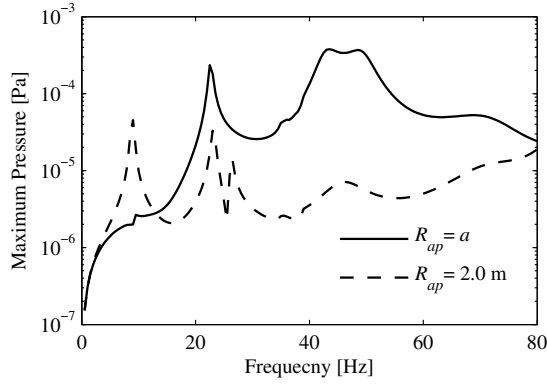
**Figure 16**. Maximum sound pressure for the optimum value of $R_{ap}$ as a result of minimising $J_{25}$
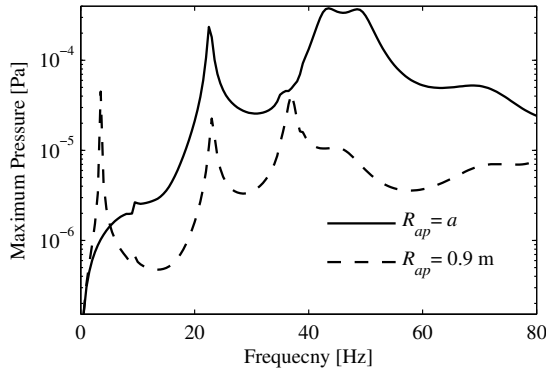


**Figure 17**. Maximum sound pressure for the optimum value of $R_{ap}$ as a result of minimising $J_{25,50,75}$

Similar results can be obtained by minimising the radiated sound power, which has been estimated at the hull surface. The sound power can be expressed as an integral over the surface of the structure $S_0$, and is given by

$$\Pi_0 = \frac{1}{2}\mathrm{Re}\int_{S_0} p_0 \dot{W}_0^* dS_0 \tag{31}$$

$\dot{W}_0$ is the surface normal velocity and the asterisk * denotes the complex conjugate. $p_0$ is the surface pressure and can be expressed in terms of an acoustic impedance $Z_a = p_0/\dot{W}_0$. Equation (31) can be rewritten as

$$\Pi_0 = \frac{1}{2}\mathrm{Re}\int_{S_0} Z_a \left|\dot{W}_0\right|^2 dS_0 \tag{32}$$

The cost function to be minimised is now given by

$$J_{W,0-f_u} = \int_0^{f_u} \Pi_0 df \tag{33}$$

The results for the variation of several cost functions with connection radius are shown in Fig. 18. It can be seen that the general trend and values of the optimum connection radii are similar to those obtained by minimising the far-field maximum sound pressure. The optimum values for the connection radius for the various cost functions are highlighted with a black spot. The optimum connection radius for minimising the full frequency range again occurs at $R_{ap} = 0.8$ m, and is very close to the optimum radius for minimising the cost function for several discrete frequencies.

Minimising the radiated sound power has the advantage in that it does not require solving the Helmholtz integral.
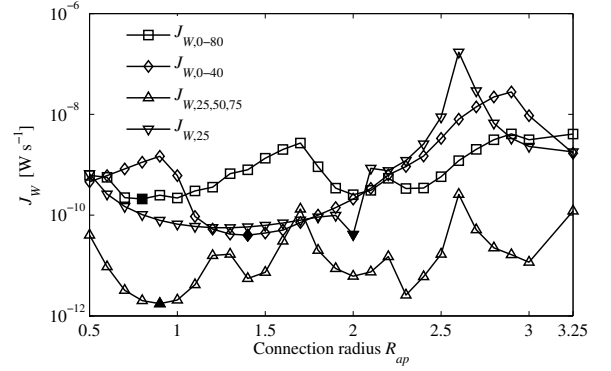


**Figure 18**. Variation of the cost function $J_W$

The frequency response function of the axial displacement at the connection between the cylindrical hull and the stern end plate is presented in Fig. 19, for the optimum connection radius of $R_{ap} = 0.8$ m and for a rigid connection corresponding to $R_{ap} = a$ when the propeller-shafting system is connected to the outer periphery of the hull. When $R_{ap} = a$, the end plate is considered rigid (Dylejko 2007; Pan et al. 2008a, 2008b; Merz et al. 2009). A much lower response is observed when the flexibility of the plate is considered. Figure 20 shows the force transmissibility between the propeller and the end plate at the hull junction, determined by $T_x = N_{x,a}/F_0$. Minimising the force transmissibility or the axial velocity at the cylinder/cone junction does not result in an optimum connection radius for minimisation of the far field radiated sound. This is due to the fact that the optimisation does not take into account the radiation efficiency of the excited modes.
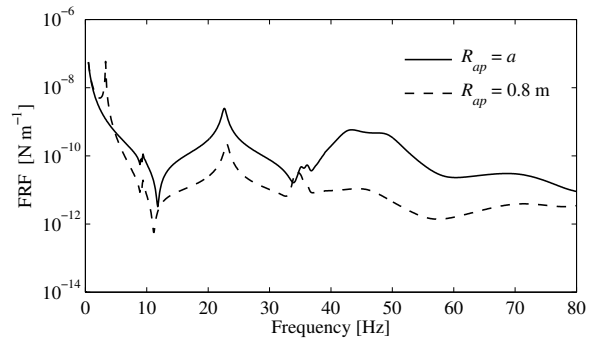


**Figure 19**. Frequency response function of the axial cylinder displacement at $x=0$ for optimum and extreme values of the connection radius.
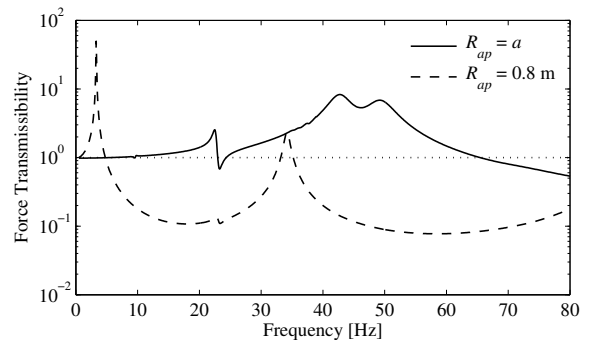


**Figure 20**. Force transmissibility for optimum and extreme values of the connection radius.

## CONCLUSIONS

A model of a propeller-shafting system coupled to a submarine hull through a flexible end plate has been presented. The submerged vessel was excited by an axial harmonic force from the propeller. Reduction of the far field radiated sound pressure was achieved using the connection radius as a tuning parameter. A cost function based on the maximum radiated sound pressure for both discrete frequencies and a specific frequency range was minimised. Minimisation of the radiated sound power at the hull surface and the radiated sound pressure gave similar results for the optimum value of the connection radius, since these quantities are directly related. The connection radius and the flexibility of the end plate were shown to be key parameters in the design of an optimum propulsion system for a submarine.

## REFERENCES

Caresta, M. and Kessissoglou, N.J. (2008) Vibration of fluid loaded conical shells. *Journal of the Acoustical Society of America*, 124, 2068-2077.

Caresta, M. and Kessissoglou, N.J. (2010) Acoustic signature of a submarine hull under harmonic excitation. *Applied Acoustics*, 71, 17-31

Dylejko, P.G. (2007) *Optimum resonance changer for submerged vessel signature reduction*, PhD Thesis, School of Mechanical and Manufacturing Engineering, The University of New South Wales, Sydney, Australia.

Fuller, C.R. (1986) Radiation of sound from an infinite cylindrical elastic shell excited by an internal monopole source. *Journal of Sound and Vibration*, 109, 259-75.

Goodwin, A.J.H. (1960) The design of a resonance changer to overcome excessive axial vibration of propeller shafting. *Transactions of the Institute of Marine Engineers*, 72, 37-63.

Hoppmann, W.H. (1958) Some characteristics of the flexural vibrations of orthogonally stiffened cylindrical shells. *Journal of the Acoustical Society of America*, 30, 77-82.

Kane, J.R. and McGoldrick, R.T. (1949) Longitudinal vibrations of marine propulsion-shafting systems. *Transactions of the Society of Naval Architects and Marine Engineers*, 57, 193-252.

Leissa, A.W. (1993) *Vibration of shells*, New York, American Institute of Physics.

Lewis, E.V. (1988) *Principles of Naval Architecture*, Jersey City, NJ, Society of Naval Architects and Marine Engineers.

Merz, S., Kinns, R. and Kessissoglou, N.J. (2009) Structural and acoustic responses of a submarine hull due to propeller forces. *Journal of Sound and Vibration*, 325, 266-286.

Pan, X., Tso, Y. and Juniper, R. (2008a) Active control of low-frequency hull-radiated noise. Journal of Sound and Vibration, 313, 29-45.

Pan, X., Tso, Y. and Juniper, R. (2008b) Active control of radiated pressure of a submarine hull. Journal of Sound and Vibration, 311, 224-242.

Parkins, D.W. and Horner, D. (1989) Active magnetic control of oscillatory axial shaft vibrations in ship shaft transmission systems, Part 1: System natural frequencies and laboratory scale model. *Journal of Tribology Transactions*, 32 170-178.

Rigby, C.P. (1948) Longitudinal vibration of marine propeller shafting. *Transactions of the Institute of Marine Engineers*, 60, 67-78.

Rosen, A. and Singer, J. (1974) Vibrations of axially loaded stiffened cylindrical shells. *Journal of Sound and Vibration*, 34, 357-78.

Schwanecke, H. (1979 ) Investigations on the hydrodynamic stiffness and damping of thrust bearings in ships. *Transactions of the Institute of Marine Engineers*, 91, 68-77.

Tso, Y.K. and Hansen, C.H. (1995) Wave propagation through cylinder/plate junctions. *Journal of Sound and Vibration*, 186, 447-461.

Tso, Y.K. and Jenkins, C.J. (2003) *Low frequency hull radiation noise*, Report No. Dstl/TR05660, Defence Science and Technology Organisation, UK.